Chapter

Study of Structural and Melting Properties of Gold Nanorods

Rida Essajai

Abstract

MD simulations combined with the embedded-atom method have been applied to study the structural and melting properties of gold nanorods (AuNRs) of different sizes. The simulation results for the actual structure of AuNRs obtained after energy minimization processes revealed that the AuNRs with largest cohesive energies tend to be structurally more stable than those with smallest ones. Then, it was found that each actual structure of AuNR is classified as an irregular structure composed of a crystalline gold core covered by an amorphous gold shell. In addition, the results showed that the melting of the AuNR surface is an inhomogeneous, gradually occurring process. Besides, it was established that the premelting ratio is inversely correlated with the AuNR size, indicating that the premelting phenomenon is more pronounced in large NP sizes than in small ones.

Keywords: gold nanorods, size effect, thermodynamic properties, melting temperature, premelting temperature, MD simulations

1. Introduction

Gold-based nanorods have attracted and continue to attract the attention of a vast amount of scientists from all over the world thanks to their fundamental and pragmatic significance. Due to their exciting properties that are found to be absent in corresponding bulk counterpart, the gold nanorods (AuNRs) are useful nanoobjects in many applications [1–14]. Especially, considerable attention has been paid over the past decades to AuNRs, because of their great importance in fabricating the new generation of nanomolecular and molecular electronics as mentioned in Ref. [15]. Besides, AuNRs can be added to base fluids in order to better improve the effective thermal properties of the nanofluids [16]. It is worth noting here that the technological properties of molecular electronic devices and the thermal property enhancement of nanofluids strongly depend on both the state of AuNR surface and temperature at which their structures change. Nonetheless, the temperature-dependent surface structure of single metal nanoparticles was ignored by several authors, where they did not take into account the surface premelting stage during the analysis of the melting process in the nanoparticles [17–19]. Therefore, it is necessary to understand the AuNR melting properties before fabricating new nanodevices based on them or suspending them in an energetic system (fluid). However, to our knowledge, the investigation on the melting properties of these nanoobjects is still lacking in the theoretical and experimental reports and, thus, needs intensive studies. To this end, the MD simulations combined with the

embedded-atom method (EAM) will be applied to study the melting behaviors of AuNRs. For this purpose, a series of results will be presented in the present work that is organized as follows: In Section 2, there is a short description of the computational method and the calculation procedure. Section 3 deals with the simulation results of AuNRs. Finally, the main conclusions arising from this work are summarized in Section 4.

2. Computational methodology

All MD simulations were performed with the LAMMPS package [20], and the atomistic visualizations were carried out by Ovito [21]. First of all, eight different model systems of rod-shaped nanoparticles were constructed using LAMMPS, where the ratio between their diameters to their lengths is more than 1:10. (Example of structure can be seen in **Figure 1.**) The detailed parameters of all rod-shaped nanoparticles are listed in **Table 1**. Furthermore, embedded-atom method (EAM) potential was adopted to describe the interatomic interaction that has been developed from the density functional theory (DFT) by Daw and Baskes [22]. Moreover, this potential has been successfully used by our group in a variety of computational disciplines [23–26]. The EAM potential used here was parameterized by Grochola et al. [27] to describe the gold–gold interactions by adjusting its parameters with experiments and ab initio calculations.

The total energy given by the EAM is written as a sum of an embedding function $F_i(\overline{\rho_i})$ and pair potential $\phi_{i,j}(r_{ij})$ as

$$E = \sum_i F_i(\overline{\rho_i}) + \frac{1}{2}\sum_{i,j}\phi_{i,j}(r_{ij}) \tag{1}$$

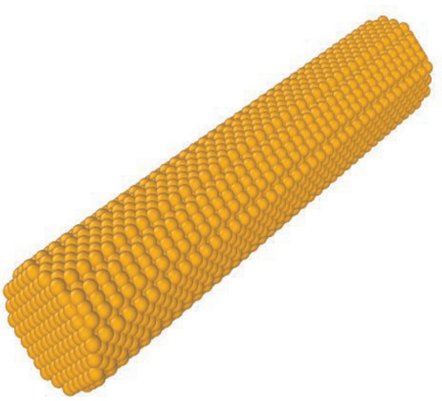

Figure 1.
Structure of rod-shaped Au nanoparticle generated by lamps (D = 6.3 nm, Lz = 61.86 nm, D:lz = 0.1, and 111147 atoms). The atomic structures are visualized by Ovito.

Nanoparticles	NP1	NP2	NP3	NP4	NP5	NP6	NP7	NP8
D (nm)	2.03	3.84	4.64	5.07	6.3	7.32	8.42	9.44
Lz (nm)	19.43	30.43	41.25	50.55	61.86	72.43	83.34	93.04
N (atoms)	8907	13,907	42,375	74,164	111,147	149,133	194,139	243,880

Table 1.
Diameter D, length lz, and total number atoms (N) for the AuNRs.

where the factor $\frac{1}{2}$ is included in order to avoid double computation of the atom couples, $r_{ij} = \left|\overrightarrow{r_j} - \overrightarrow{r_i}\right|$ is the scalar distance, and $\overline{\rho_i}$ is the host electron density induced by all encirclement atoms j at the position of atom i. The host electron density is given by

$$\overline{\rho}_i = \sum_{i \neq j} \rho_i(r_{ij}) \tag{2}$$

In order to investigate the melting properties of AuNRs of different sizes, a series of MD simulations were carried out. First, all models considered in this work are equilibrated over 500,000 time steps in the NVT ensemble at zero temperature using the velocity Verlet method with a fixed time step of 1 fs and neglecting the periodic boundary conditions (PBCs) in three dimensions. Then after energy minimization process, the actual model systems at 0 K were obtained and characterized using two structural techniques, namely, the coordination number (CN) analysis and the common neighbor analysis (CNA) method. The final point of the simulations is that all the simulated equilibrium samples are heated by increasing the temperature from 0 to 2300 K using NVT.

In order to predict the melting temperatures of AuNRs, the variation of thermodynamic properties (including the potential energy per atom (U) and the heat capacity (C)) with respect to temperature was analyzed. The heat capacity is obtained from the ensemble averages of U and its square, as [28]

$$\frac{C}{K_B} = \frac{1}{NK_B^2T^2}\left(\langle U^2\rangle - \langle U\rangle^2\right) + \frac{3}{2} \tag{3}$$

where T is the temperature, N is the number of atoms, and K_B is the Boltzmann constant.

Besides the thermodynamic properties, the melting temperature of NPs is also explored by analyzing the variation in other physical quantities in terms of the temperature [29]. In this context, the Lindemann index is regarded as one of the most important of these quantities. Additionally, this index is a tool to examine the NP in the layer form in order to determine from where the NP melting begins. The Lindemann index of each layer, $\delta_{L(i)}$, is represented as [30]

$$\delta_{L(i)} = \frac{2}{N_{L(i)}\left(N_{L(i)} - 1\right)} \sum_{j<k} \frac{\sqrt{\langle r_{jk}{}^2\rangle - \langle r_{jk}\rangle^2}}{\langle r_{jk}\rangle} \tag{4}$$

where $L(i)$ is the *ith* layer, r_{jk} is the distance between atoms k and j, $N_{L(i)}$ is number of atoms of the *ith* layer, and the bracket $\langle\rangle$ represents the ensemble average.

3. Results and discussions

Although the initial structures of gold nanorods can be generated by using LAMMPS, these original structures are not the nanorods with equilibrium states (i.e., metastables). Therefore, it is necessarily to get the actual model systems (i.e., the real calculation models) before studying the structural analysis.

Using the MD simulation, the temporal evolution of each nanostructure passes through several states until it reaches a more stable one, corresponding to minimum

total energy, but remains metastable, resulting from its surface atoms always wanting to aggregate to reduce surface energy as was indicated in Ref. [5]. After this pretreatment stage, the structure stability of AuNRs was investigated by the size-dependent cohesive energy (the absolute value of total energy) of the AuNR, and the results were plotted in **Figure 2**.

As expected, it is found that the calculated cohesive energies of the particles are lower than that of the bulk Au which was obtained previously [23, 31]. It was also established that the cohesive energy of AuNR is very sensitive to the size. The cohesive energy value increases with increasing AuNR size. This behavior seems to indicate that the AuNRs of higher energies tend to be structurally more stable and it can be explained in terms of reducing the influence of surface free energy (i.e., energy of all of the dangling bonds in the surface) resulting from the decrease in the dangling bonds to total bonds ratio when increasing the size.

Within the framework of the local structural characterization of AuNRs, the common neighbor analysis (CNA) technique was adopted. For more details on this method, see Refs. [23, 32, 33]. Once AuNRs in their equilibrium states were obtained (see **Figure 3a** which displays the section of [100]-oriented equilibrium AuNR at different sizes), the two categories of Au atoms in each NR were calculated by the CNA technique; then their percentage were illustrated in **Figure 3b**. It was found from **Figure 3b** that for the smallest AuNR (D = 1.622 and Lz = 15.26 nm), there is a significant percentage of unidentified structures (47.5%), while proportion of *fcc* structures is identified by 52.5%. It was moreover observed that for all AuNR sizes, the fraction of Au atoms having *fcc* structures is higher than those possessing unidentified structures. Also, it was found that when the AuNR size increases, the fraction of both the *fcc* structure and unidentified one are, respectively, an increasing and decreasing function until they reach percentages of 82.5 and 17.5% at size correspondent to D = 8.704 nm and Lz = 86.12 nm (NP8).

In order to describe in more details the local atomic-level structures in different size of AuNRs, the coordination number (CN) about each individual atom was calculated; then the results are presented in **Figure 4**. It was shown that each actual structure of the AuNR obtained after energy minimization process reveals the core-shell structure composed by a crystalline gold core (full-coordinated atoms with the CN = 12) covered by an amorphous gold shell. This last part is divided into two

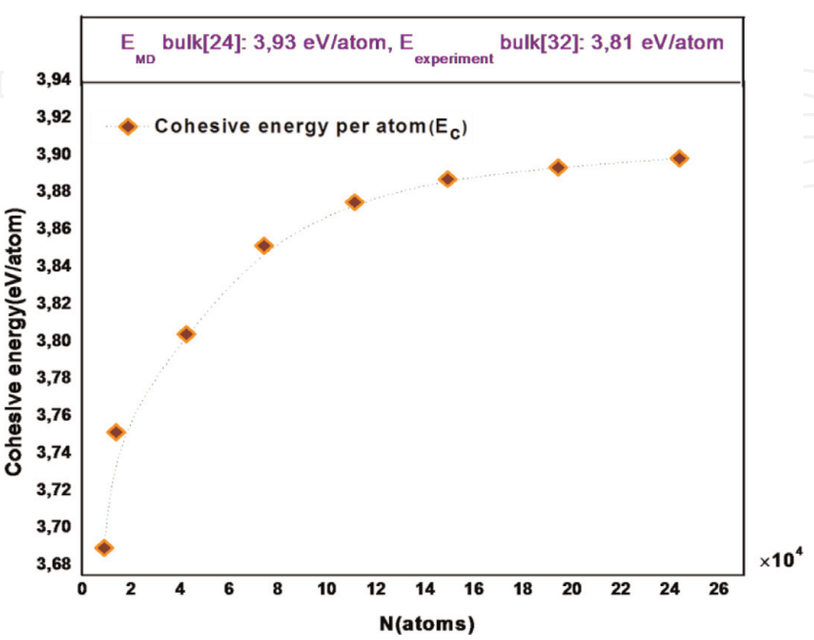

Figure 2.
The cohesive energy per atom as a function of the AuNR size (N) after energy minimization.

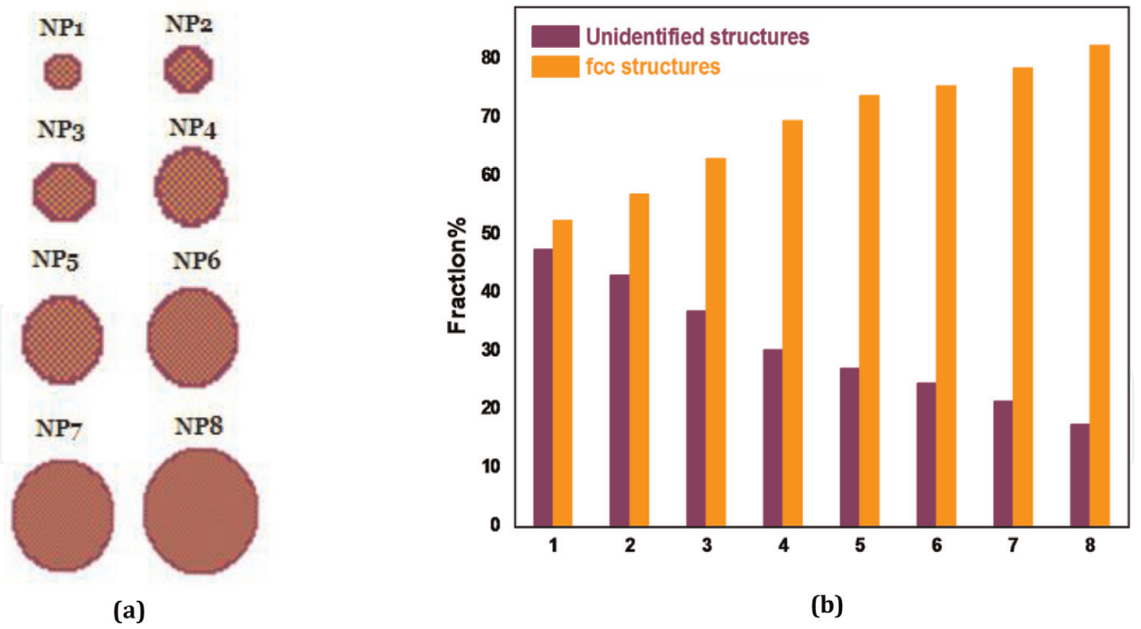

Figure 3.
(a) Sections of [100]-oriented AuNRs after energy minimization. (b) The atomic structures are visualized by Ovito. The percentage of each category of atoms in AuNRs is counted by using the CNA method, yellow for fcc structures and purple for unidentified structures.

layers: the first contains atoms located on the subsurface layer (CN = 11 and 10), the second consists of atoms located on the free-surface layer, corresponding to both low-index facets [i.e., {110} and {100} facets with the CN = 7 and CN = 8 and their perimeter (edge and corner with the CN < 7)]. Apparently, the shell part of the NP is inherently different from the core one, where its atoms possess structure intermediate between the bulk liquid structure and the bulk solid one. It is worth mentioning that the classification of AuNRs in core-shell constructions obtained here supports the previous experimental and simulated studies carried out on single metal nanoparticles [23–26, 34, 35]. Furthermore, it was seen from **Figure 4** that for all simulated AuNRs, the fraction of liquid-like atoms located in the shell part is smaller than that of solid-like atoms located in the core part. It was also found that for all actual structures of AuNRs, the liquid-like atoms located in the area of low-index facets (7 and 8 coordinated atoms) exhibit the highest fraction in the shell part. In addition, when the AuNR size increases, the fraction of atoms' core part increases from 51 to 83%, while the total fraction of shell atoms decreases from 49 to 17%. These findings are consistent with those previously reported by the CNA analysis. The results of the current study indicates that the ratio of low-coordinated atoms to full-coordinated atoms is inversely correlated with the AuNR size.

Figure 5 shows the typical trend of potential energy (U) and heat capacity (C) of different AuNR sizes as a function of temperature T during the heating process from 0 to 2300 k. For each AuNR, it was established that the U curve presents a jump at the same temperature that the C curve has a sharp peak corresponding to the complete melting point (T_{pm}) of the AuNR (observed at 1270.17 K for NP1, 1306.43 for NP2, 1330.34 for NP3, 1349.18 for NP4, 1361.85 for NP5, 1367.07 for NP6, 1372.52 for NP7, and 1377.65 K for NP8). As predicted, the results observed here reveal that the complete melting points of AuNRs are lower than that of bulk Au obtained previously [23, 36]. It was also found that, as the AuNR size increases, the simulated value of T_{pm} increases. This behavior is in agreement with previous results [37, 38]. Notably, the increase of T_{pm} could be attributed to the decrease in the ratio of low-coordinated atoms to full-coordinated ones (i.e., the total number

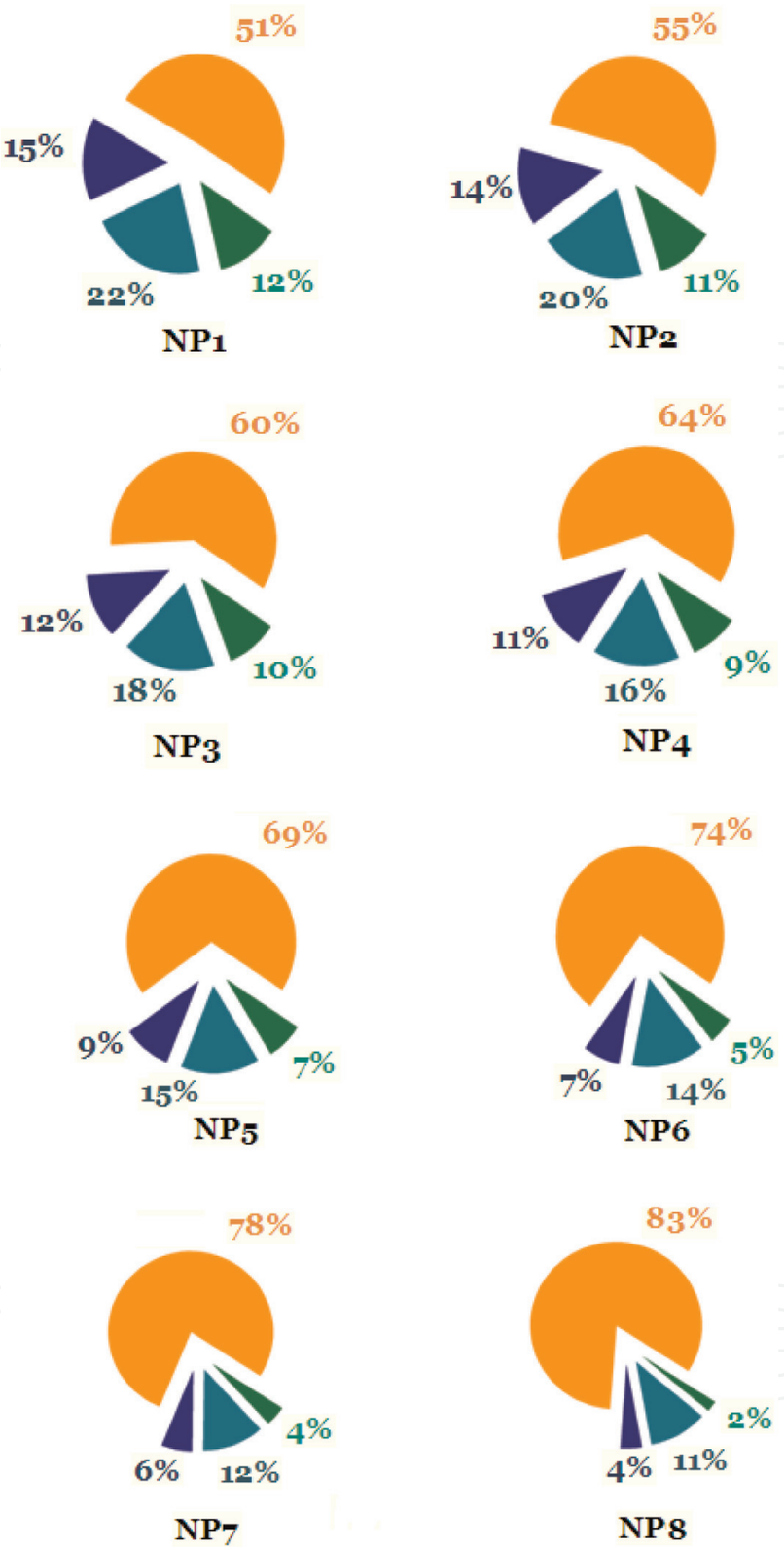

Figure 4.
The distribution of the coordination numbers of AuNR for different sizes, orange for fcc *structures, royal for second layer (CN = 11, 10), olive for Perimeter atoms (CN < 7), and dark cyan for facet atoms (CN = 7, 8).*

of bonds in the NP increases); hence, AuNRs with large sizes require more temperature to completely melt than those with small sizes.

Now we will turn to **Figure 6**, which shows the temperature-dependent Lindemann index value of free-surface atoms (δ_L) for different AuNR sizes. It is easy to see that in the beginning of the heating process, the δ_L increases slowly and linearly, thus suggesting that all surface atoms merely vibrate around their original

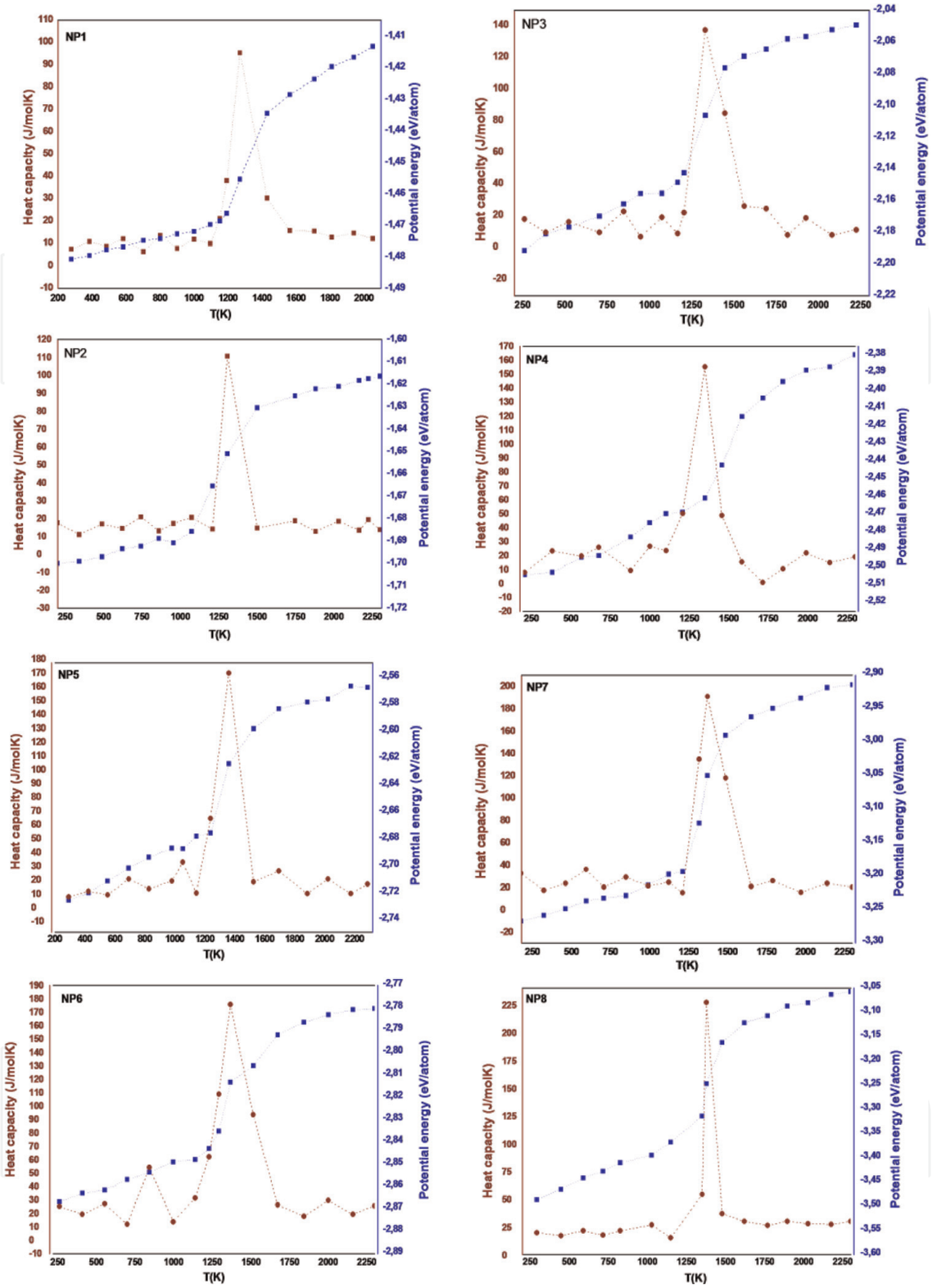

Figure 5.
Variation of the heat capacity and potential energy per atom of AuNR for different sizes, during the heating process.

lattice positions. Then, δ_L abruptly jumped, and its factor is many times greater than before, from which the premelting phenomenon occurs at the temperature before that of complete melting; hence some liquid-like atoms start to appear. It is evident that after the sharp rise, δ_L increased with fluctuations at several temperatures. This latter can be ascribed to the nonhomogeneous nature of the melting of free-surface atoms originating from the coexistence between two types of atoms: those who are moving and those who are remaining strongly constrained in their solid ordering

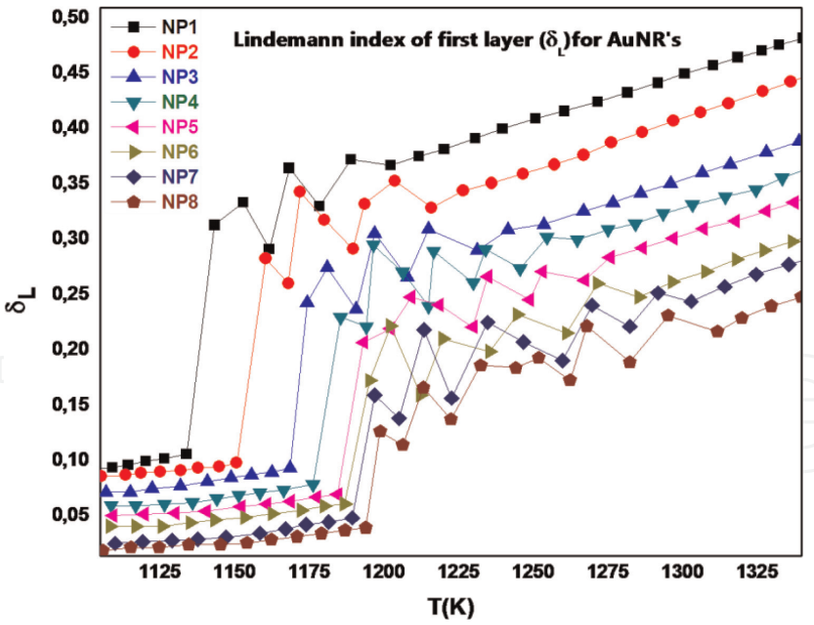

Figure 6.
Temperature-dependent Lindemann index of first layer for AuNRs.

against premelting phenomenon. Besides, it was observed that the fluctuations presenting in δ_L curve are attenuated progressively with the increase in temperature until completely damped. This may be due to the increased amount of liquid-like atoms until they form a continuous liquid layer. It can be clearly shown from **Figure 6** that the higher temperature region where δ_L increases monotonically is in the liquid-like range of the first layer for AuNR different sizes. This liquid region of δ_L curve may correspond with the fact that all surface atoms moved cooperatively.

Once again according to **Figure 6**, the onset of premelting temperature (T_{sm}) of each actual structure of the AuNR is determined from the temperature where δ_L curve shows a sharp increase. The results showed that T_{sm} decreased from 1198.82 K for NP8 to 1142.87 K for NP1, and considering the T_{pm} already determined from U and C curves (**Figure 5**), its value is above the T_{sm} one. It was also found that the T_{sm}value decreased by 177.51 for NP8, 174.17 for NP7, 170.57 for NP6, 165.40 for NP5, 159.25 for NP4, 151.98 for NP3, 139.18 for NP2, and 127.3 for NP1, compared with the T_{pm} one. On the basis of the above, it was concluded that all AuNRs in the present study are passing through the surface premelting stage during heating process.

Our attention will now be drawn to identifying how the ratio between T_{sm} and T_{pm} of AuNR also called the premelting ratio varies in terms of size. One of the main objectives of this investigation is to provide insights into the AuNR size-dependent premelting phenomenon. Hence, this study aims to fill this void in the existing literature. **Figure 7** is given to show the behavior of the premelting ratio of AuNR as a function of the size (N). It was found that the premelting ratio value decreases when the NP size increases, thus indicating that the premelting phenomenon is less pronounced in small NP sizes than in large ones.

4. Conclusions

In summary, the structural and melting properties of AuNRs have been investigated by means of MD simulations combined with the embedded-atom method (EAM) potential. The simulation results for the actual structure of AuNRs revealed

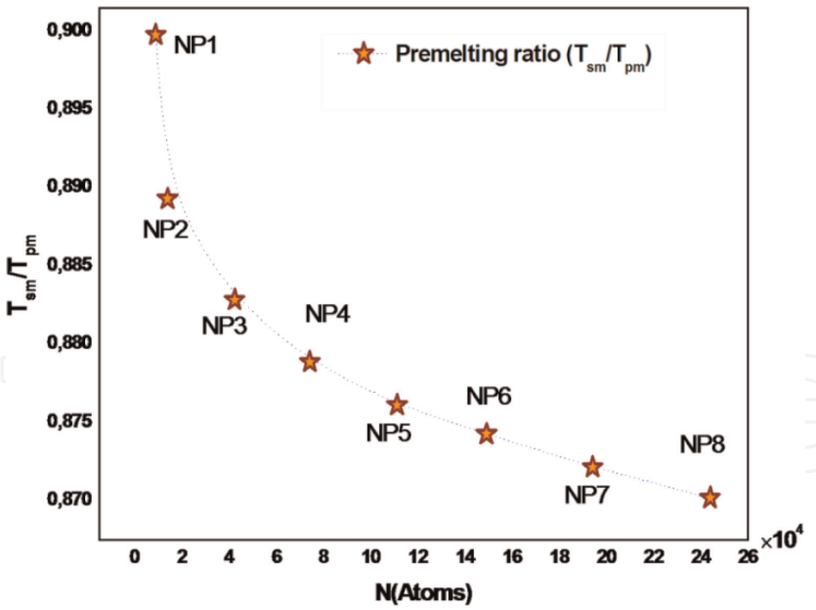

Figure 7.
Premelting ratio as a function of the particle size (N).

that AuNRs of smaller cohesive energies tend to be structurally less stable than those larger ones. Then, the local structure characterization of the actual structure of AuNRs carried out by using the CN and CNA techniques showed that each AuNR is classified as an irregular structure which is composed of a crystalline gold core that is covered by an amorphous gold shell. Further, it was shown that melting temperatures of the actual structure of AuNRs are below that in bulk state. In addition, it was found that the surface melting in the actual structure of AuNRs is an inhomogeneous, gradually occurring process. Besides, the result of the size-dependent premelting ratio proved that the premelting phenomenon is less pronounced in small AuNRs than in large ones.

Author details

Rida Essajai
Group of Semiconductors and Environmental Sensor Technologies- Energy Research Center, Faculty of Science, Mohammed V University, Rabat, Morocco

*Address all correspondence to: rida.essajai@gmail.com

References

[1] Yu-Ying Y, Chang S-S, Lee C-L, Chris Wang CR. Glod nanorods: Electrochemical synthesis and optical properties. The Journal of Physical Chemistry. B. 1997;**101**(34):6661-6664

[2] Hu H, Reven L, Rey A. First-principles density functional theory (DFT) study of glod nanorod and its interaction with alkanethiol ligands. The Journal of Physical Chemistry. B. 2013; **117**:12625-12631

[3] Huang X, Neretina S, El-Sayed MA. Glod nanorods: From synthesis and properties to biological and biomedical applications. Advanced Materials. 2009; **21**:4880-4910

[4] Murphy CJ, Gole AM, Stone JW, Sisco PN, Alkilany AM, Goldsmith EC, et al. Gold nanoparticles in biology: Beyond toxicity to cellular imaging. Accounts of Chemical Research. 2008; **41**:1721-1730

[5] Qiu Y, Liu Y, Wang L, Xu L, Bai R, Ji Y, et al. Surface chemistry and aspect ratio mediated cellular uptake of Au nanorods. Biomaterials. 2010;**31**: 7606-7619

[6] Huang X, El-Sayed IH, Qian W, El-Sayed MA. Cancer cells assemble and align glod nanorods conjugated to antibodies to produce highly enhanced, sharp, and polarized surface Raman spectra: A potential cancer diagnostic marker. Nano Letters. 2007;**7**:1591-1597

[7] Durr NJ, Larson T, Smith DK, Korgel BA, Sokolov K, Ben-Yakar A. Two-photon luminescence imaging of cancer cells using molecularly targeted glod nanorods. Nano Letters. 2007;**7**: 941-945

[8] Huff TB, Tong L, Zhao Y, Hansen MN, Cheng JX, Wei A. Hyperthermic TEMPeffects of gold nanorods on tumor cells. Nanomedicine. 2007;**2**:125-132

[9] Milette J, Toader V, Reven L, Lennox RB. Tuning the miscibility of gold nanoparticlesdispersed in liquid crystals *via* the thiol-for-DMAPreaction. Journal of Materials Chemistry. 2011;**21**: 9043-9050

[10] Liao Q, Mu C, Xu DS, Ai XC, Yao JN, Zhang JP. Glod nanorod arrays with good reproducibility for high-performance surface-enhanced Raman scattering. Langmuir. 2009;**25**: 4708-4714

[11] Singh AK, Senapati D, Wang S, Griffin J, Neely A, Candice P, et al. Gold nanorod based selective identification of *Escherichia coli* bacteria using two-photon Rayleigh scattering spectroscopy. ACS Nano. 2009;**3**: 1906-1912

[12] Nappa J, Revillod G, Abid JP, Russier-Antoine I, Jonin C, Benichou E, et al. Hyper-Rayleigh scattering of gold nanorods and their relationship with linear assemblies of gold nanospheres. Faraday Discussions. 2004;**269**:935-939

[13] Durr NJ, Ericson MB, Ben-Yakar A. Multiphoton luminescence from gold nanoparticles as a potential diagnostic tool for early cancer detection. In: Herold KE, Rasooly A, editors. Biosensors and Molecular Technologies for Cancer Diagnostics. Oxford: Taylor & Francis; 2012. pp. 307-322. DOI: 10.1080/00107514.2013.766641.ch17

[14] Oldenburg L, Hansen MN, Zweifel DA, Wei A, Boppart SA. Plasmon-resonant gold nanorods as low backscattering albedo contrast agents. Optics Express. 2006;**14**:6724-6738

[15] Service RF. Breakthrough of the year. Molecules get wired. Science. 2001;**294**:2442

[16] Jeon J, Park S, Lee BJ. Optical property of blended plasmonic

nanofluid based on glod nanorods. Optics Express. 2014;**22**:1101-1111

[17] Fang K-C, Weng C-I, Ju S-P. An investigation into the structural features and thermal conductivity of silicon na noparticles using molecular dynamics simulations. Nanotechnology. 2006;**17**: 3909-3914

[18] Nanda KK, Sahu SN, Behera SN. Liquid-drop model for the size-dependent melting of low-dimensional systems. Physical Review A. 2002;**66**: 013208

[19] Shi FG. Size dependent thermal vibrations and melting in nanocrystals. Journal of Materials Research. 1994;**9**: 1307-1313

[20] LAMMPS Users Manual 30. Sandia National Laboratories; 2 Oct 2014

[21] Stukowski A. Visualization and analysis of atomistic simulation data with OVITO–the open visualization tool. Modelling and Simulation in Materials Science and Engineering. 2010;**18**:015012

[22] Daw MS, Baskes MI. Embedded-atom method: Derivation and application to impurities, surfaces, and other defects in metals. Physical Review B. 1984;**29**:6443

[23] Essajai R, Hassanain N. Molecular dynamics study of melting properties of gold nanorods. Journal of Molecular Liquids. 2018;**261**:402-410

[24] Essajai R, Rachadi A, Feddi E, Hassanain N. MD simulation-based study on the thermodynamic, structural and liquid properties of gold nanostructures. Materials Chemistry and Physics. 2018;**218**:116-112

[25] Erko S. Physica E. 2000;**8**:210-218

[26] Qi W. Nanoscopic thermodynamics. Accounts of Chemical Research. 2016; **49**(9):1587-1595

[27] Grochola G, Russo SP, Snook IK. On fitting a gold embedded atom method potential using the force matching method. The Journal of Chemical Physics. 2005;**123**:204719

[28] Bagrets A, Werner R, Evers F, Schneider G, Schooss D, Wölfle P. Lowering of surface melting temperature in atomic clusters wif a nearly closed shell structure. Physical Review B. 2010;**81**:075435

[29] Kart HH, Yildirim H, Ozdemir KS, Cagin T. Physical properties of Cu nanoparticles: A molecular dynamics study. Materials Chemistry and Physics. 2014;**15**:204-212

[30] Yang Z, Yang X, Xu Z. Molecular dynamics simulation of the melting behavior of Pt−Au nanoparticles with core−shell structure. Journal of Physical Chemistry C. 2008;**112**:4937-4947

[31] Kittel C. Introduction to Solid State Physics. 5th ed. New York: Wiley; 1976

[32] Wu L, Zhang Y, Wen Y-H, Zhu Z-Z, Sun S-G. Molecular dynamics investigation of structural evolution of fcc Fe nanoparticles under heating process. Chemical Physics Letters. 2011; **502**:207-210

[33] Stukowski A. Structure identification methods for atomistic simulations of crystalline materials. Modelling and Simulation in Materials Science and Engineering. 2012;**20**:45021

[34] Huang WJ, Sun R, Tao J, Menard LD, Nuzzo RG, Zuo JM. Coordination-dependent surface atomic contraction in nanocrystals revealed by coherent diffraction. Nature Materials. 2008;**7**:308

[35] Qi W, Huang B, Wang M. Structure of unsupported small palladium nanoparticles. Nanoscale Research Letters. **4**(3):269-273

[36] Shim J-H, Lee B-J, Cho YW. Thermal stability of unsupported glod nanoparticle: a molecular dynamics study. Surface Science. 2002;**512**: 262-268

[37] Qi WH. Size TEMPeffect on melting temperature of nanosolids. Physica B. 2005;**368**:46-50

[38] Buffat Ph, Borel J-P. Size effect on the melting temperature of gold particles. Physical Review A. 1976;**13**: 2287